Ground thermal and geomechanical conditions in a permafrost-affected high-latitude rock avalanche site (Polvartinden, northern Norway)

Regula Frauenfelder[1], Ketil Isaksen[2], Jeannette Noetzli[3], Matthew J. Lato[4]

[1]Norwegian Geotechnical Institute NGI, Oslo, 0806 Norway
[2]The Norwegian Meteorological Institute, Oslo, 0313, Norway
[3]Formerly University of Zurich, Zurich, 8057, Switzerland, now at: WSL-Institute for Snow and Avalanche Research SLF, Davos, 7260, Switzerland
[4]Formerly NGI, now at: BGC Engineering Inc., Ottawa ON, Canada

Correspondence to: R. Frauenfelder (rf@ngi.no)

Abstract. On June 26, 2008, a rock avalanche detached in the northeast facing slope of Polvartinden, a high-alpine mountain in Signaldalen, northern Norway. Here, we report on the observed and modelled past and present near-surface temperature regime close to the failure zone, as well as on a subsequent simulation of the subsurface temperature regime, and on initial geomechanical mapping based on laser scanning. The volume of the rock avalanche was estimated to be approximately 500'000 m^3. The depth to the actual failure surface was found to range from 40 m at the back of the failure zone to 0 m at its toe. Visible in-situ ice was observed in the failure zone just after the rock avalanche. Between September 2009 and August 2013 ground surface temperatures were measured with miniature temperature data loggers at fourteen different localities close to the original failure zone along the northern ridge of Polvartinden, and in the valley floor. The results from these measurements and from a basic three-dimensional heat conduction model suggest that the lower altitudinal limit of permafrost at present is at 600-650 m a.s.l, which corresponds to the upper limit of the failure zone. A coupling of our in-situ data with regional climate data since 1958 suggests a general gradual warming and that a period with highest mean near surface temperatures on record ended four months before the Signaldalen rock avalanche detached. A comparison with a transient permafrost model run at 10 m depth, representative for areas where snow accumulates, strengthen this findings, which are also in congruence with measurements in nearby permafrost boreholes. It is likely that permafrost in and near the failure zone is presently subject to degradation. This degradation, in combination with the extreme warm year antecedent to the rock failure, is seen to have played an important role in the detaching of the Signaldalen rock avalanche.

1 Introduction

In the morning of June 26th, 2008 a rock avalanche (cf. Hungr et al., 2014 for nomenclature) detached from the northeast facing slope of Polvartinden, a 1275 m high mountain in Signaldalen, Troms county, northern Norway (located at

69°10'18"N/19°57'47"E; Fig. 1). The rock avalanche endangered two farms and several recreation cabins, and it destroyed a considerable amount of livestock pastures. Just after the event, first reconnaissance work was carried out, including failure zone assessment by means of visual inspection from a helicopter. During this visual inspection, a few hours after the event, in-situ ice was observed in the failure zone at several meters depth (Fig. 2), i.e., clearly indicating permafrost. This observation, together with the absence of any typical pre-weather conditions (such as intensive rainfall or snow melt) that could have triggered the rock avalanche, led to the hypothesis that warming or degrading of permafrost could have played a role in the timing and the magnitude of the event. A year after the event, a temporary temperature monitoring network was put in place and repeated surveying of the failure zone and the adjacent slopes by means of terrestrial laser scanning was initialized.

Scientists have become increasingly aware that atmospheric warming has a potential impact on mountain permafrost (e.g., Haeberli, et al., 2010; Harris et al., 2009; Jin et al., 2000; Marchenko et al., 2007; Stoffel and Huggel, 2017). It seems that mountain systems are especially sensitive to a changing climate due to feedback effects in connection with snow cover, albedo and heat budgets, which amplify the alterations caused by climate change (Gobiet et al., 2014; Vavrus 2007; Wang et al., 2014). Several studies from the European Alps show that temperatures have increased twice as much as the global average since around 1900. There is also increasing evidence that there exists a link between rockfall magnitude and frequency, and timing and depth of permafrost degradation, the latter ranging from seasonal increase of active-layer depths to long-term, deep-seated warming of the permafrost body as a response to atmospheric temperature rise (e.g., Gruber and Haeberli, 2007; Ravanel and Deline, 2010). Fischer et al. (2012) collected published material on large rock avalanche and rock avalanche events (volumes between 10^5 and 10^7 m^3), as well as on more frequent small-volume rockfall events. Their study concludes that such events occur worldwide in periglacial environments, and that many of the reviewed studies suggest that the reported events may be related to ongoing and/or past changes in permafrost and glacierization. Corresponding events have, for example, been documented for the European Alps (e.g., Barla et al., 2000; Crosta et al., 2004; Gruber et al., 2004; Cola, 2005; Deline et al., 2011; Oppikofer et al., 2008; Ravanel and Deline, 2010; Phillips et al., 2016), Canada and Alaska (e.g., Evans and Clague, 1994; Geertsema et al., 2006), the Caucasus (e.g., Haeberli et al., 2004) and for New Zealand (e.g. Allen et al., 2011).

In mainland Norway (i.e., excluding Svalbard), permafrost occurs mainly in the central mountain chains and in higher latitude areas, such as the counties of Troms and Finnmark (Gisnås et al., 2016). Early studies by, e.g., King (1986), Ødegård et al. (1996), and Etzelmüller et al. (2003) have shown that permafrost is discontinuous in the higher mountains of central southern and eastern Norway. More recent studies (e.g., Farbrot et al., 2011) yield that permafrost temperatures in general are between -3 and 0°C in the higher mountains of southern Norway and warming and degrading permafrost have been documented to occur at sites with cold permafrost, marginal permafrost and deep seasonal frost (Isaksen et al., 2011). It has, therefore, to be expected that the permafrost is particularly vulnerable to climate change (Christiansen et al., 2010; Farbrot et

al., 2011). Large-scale rock-slope failures pose a significant geohazard in the fjords and valleys of western and northern Norway (Blikra et al., 2006). A study by Blikra and Christiansen (2014) on the interactions between permafrost and rock avalanche deformation at the Nordnesfjellet site in northern Norway (location indicated in Fig. 1) shows that systematic seasonal changes – thought to be controlled by sporadic permafrost occurrence – considerably affect the shear strength of the sliding planes (Blikra et al., 2015).

Only few studies are available on the distribution of mountain permafrost and its thermal state in high-relief areas in northern Norway. Due to increased awareness of the potential role of permafrost degradation to landslide risk, a permafrost and climate monitoring programme was initiated in 2002, along climate and altitudinal transects in Troms and Finnmark, the two northernmost counties of mainland Norway (Isaksen et al., 2008; Farbrot et al., 2013). In 2003, a permafrost programme was launched in the Gaissane Mountains in northernmost county Finnmark (Farbrot et al., 2008). In the mountains of Troms two 30–32 m deep boreholes were drilled in 2004 at altitudes of 786–850 m asl (Farbrot et al., 2013). These studies found permafrost to be warm, but widespread in alpine areas in northern Norway. The existing monitoring network in northern Norway was more extensively instrumented and extended with new boreholes in Troms and Finnmark during the third International Polar Year 2007–2009 (cf. Christiansen et al., 2010; Juliussen et al., 2010). Through extensive analyses of these borehole data, Farbrot et al. (2013) found that the combined effects of snow depth and vegetation cover are the two most critical factors for the existence of permafrost in northern Norway. They also concluded that the depth of seasonal frost or active layer in areas underlain by exposed bedrock was more than 10 m at several sites and was amongst the deepest reported in the international literature, and that the altitude of the lower limit of permafrost has probably increased around 200–300 m since the end of the Little Ice Age (LIA) (Farbrot et al., 2013). This was supported in a recent study by Myhra et al. (2015) who modelled permafrost distribution and long-term thermal changes in, among others, a steep rock wall at Revdalsfjellet which is situated close to the unstable and extensively monitored Nordnesfjellet (Blikra and Christiansen, 2014) and 25 km from our Signaldalen site. For the same mountain Myhra et al. (2015) modelled a bedrock warming at 20 and 50 m depth of about 1.0 and 0.5°C, respectively, from the end of the LIA and using a present lower limit of permafrost of about 650 m asl From the development of a new Nordic permafrost map there exist new modelling results, which confirm ongoing degradation of mountain permafrost in the fjord areas in Troms (Gisnås et al., 2016).

In this paper, we present analyses of a four-year temperature data series from near-surface temperature loggers, subsequent temperature regime modelling, and basic geomechanical mapping in Signaldalen, northern Norway, at a high-latitude, high-relief rock avalanche site. The main objective of our study is to increase our understanding of the permafrost temperature regime at the site and what role the ground temperatures might have played in the release of the rock avalanche. Further, we aim to contribute to the understanding of the influence of solar radiation on near surface temperatures in different aspects of steep mountain walls at high-latitudes.

2 Methods

In order to map the thickness and the geometrical characteristics of the failure zone, the release area was repeatedly surveyed by terrestrial laser scanning (TLS). This allowed also for monitoring of eventual continued or new movement in the slope.

In-situ measurements of ground surface temperatures and subsequent temperature modelling was employed to get insight into the past- and present temperature regime at and near Polvartinden peak. The larger area around the failure zone, outside the steepest slope, is characterized by a combination of small vertical rock outcrops and undulating slopes with an established soil cover. Snow cover and snow depth therefore varies considerably in these two different types of topographies. Consequently, temperature loggers were installed in both types of terrain, i.e., in both vertical rock outcrops (Fig. 3a; rock surface temperature (RST)) and within soil material of the more gentle slopes (soil surface temperature (SST)). The locations of the temperature logger placements (Fig. 3b) were also selected in order to cover different aspects.

To obtain a robust estimate of how past and present ground temperatures had evolved prior to the failure, i.e., in the long- and in the short-term, two different approaches were used: Firstly, the RST in selected rock outcrops were linked to long-term changes in regional air temperature by comparing their statistical relation with temperature data from the official weather stations Skibotn (5 m asl) and Ripojavri (502 m asl); for locations see Figure 1. We found that the linkage between those two datasets was strongest for rock outcrops with little or no snow, i.e., with a fairly direct link to the atmospheric conditions. Therefore, and secondly, it was desirable to look further into the temperature development in the ground in more gentle slope areas close to the release area with a more established snow and soil cover. To this aim, the CryoGrid2 model (cf. Westermann et al., 2013) was used. Since Polvartinden is an alpine peak, with three-dimensional effects that affect the ground temperature field inside the mountain, the lower permafrost limit will vary according to different aspects. In order to better understand the present subsurface temperature field of Polvartinden and to get a better idea of how the lower permafrost limit is located with respect to the release area of the rock avalanche, a stationary three-dimensional transient heat conduction model (cf. Noetzli et al., 2007a, b) was used in addition. It was natural to install loggers in different compass directions to study the differences in surface temperature as a result of aspect dependency. As input data for the analyses of aspect dependency robust estimates of air temperature were needed for each of the installed rock wall localities. This in order to calculate the temperature difference (ΔT) between calculated air temperature and measured rock face temperatures (surface offset).

2.1 Geomechanical mapping

In the autumns of 2010, 2011 and 2013, the failure zone of the rock avalanche was imaged with an HD Optech ILRIS terrestrial laser scanner (Optech Incorporated, Canada). In addition, the failure zone and its surroundings were imaged with a Giga-Pan camera in autumn 2013. The purpose of the laser scanning data collection was to develop a digital terrain model in

order to enable the quantification of the extent and volume of the failure zone. The data needed to be of significant resolution to enable temporal modelling of the area and identify zones that show differential movement.

The failure zone is located approximately 600 m above the valley bottom, on the western side (facing east). The altitude of the failure zone in combination with the slope of the mountain side resulted in the failure zone being located approximately 800–1100 m away from the nearest possible scanning locations. To produce a 3D terrain model with a minimal amount of occlusion data was collected from three independent locations (identified in Fig. 3b). Each location was selected because it provided an excellent line-of-sight to the failure zone and reduced the bias in extraction of discontinuity orientations in accordance with Lato et al. (2010). Data was collected at varying resolutions. Low resolution data was collected to enable the visualization and modelling of a large area of the mountainside. Higher resolution data was collected at specific zones near the failure zone and its surrounding areas to enable a geomechanical interpretation. The orientation of structural discontinuities were manually identified and orientation vectors were converted to dip and dip direction measurements (Lato et al., 2012). The structural measurements were extracted from a 3D surface mesh was generated from the overlapping point cloud datasets.

Calculating the volume of the failed mass was completed based on interpolation and estimation. Since there does not exist a sufficiently high resolution 3D image of the area before the failure, an interpolated surface had to be used to estimate the volume. The volume estimation was completed using both PolyWorks and ArcGIS software packages. The volume of the 2008 rock avalanche was computed using the 2012 TLS data by delineating a pre-failure surface based on adjacent slope topography bounding the scarp. The differential volume between the 2012 TLS data and the pre-failure surface was computed using standard 3-dimensional techniques, as presented, e.g., by Lato et al. (2014).

2.2 Ground surface and air-temperature measurements

Ground surface temperatures were measured at fourteen locations employing miniature temperature data loggers of three different types: M-Log5W loggers (GeoPrecision GmbH, Germany), redesigned UTL-1 loggers (University of Bern and University of Zurich, Switzerland, cf. Gruber et al., 2003) and UTL-3 loggers (GEOTEST and WSL Institute for Snow and Avalanche Research SLF, Switzerland). We followed the installation setup described by Gruber et al. (2003), hence measuring near-surface rock temperatures at 10 cm depth (Fig. 3a). The absolute accuracy for all three logger types is ± 0.1°C. The resolution of M-Log5W, UTL-3 and UTL-1 is 0.01, 0.02 and 0.27°C respectively. The M-Log5W loggers and the UTL-3 loggers were programmed to measure every 30 minutes, while the UTL-1 loggers (having smaller memory capacities than the other two employed logger types) measured every two hours. Based on experiences from long-term permafrost monitoring programs in Norway using such loggers (e.g., Isaksen et al., 2011; Gisnås et al., 2016) we claim that the bias on the accuracy of the temperature measurements introduced with the given setups is negligible.

Installation sites for RST were chosen based on the availability of near-vertical rock outcrops, their closeness to the original failure zone and, last but not least, the accessibility of the identified locations. Where possible, a vertical distance of several meters to the flat terrain was chosen, however, this was not possible at all of the sites, which has some implications on the interpretation of the results (cf. chapter 4). The fourteen measurement sites finally chosen are plotted on the map shown in Fig. 3b; they are located along the NNW-ridge of Polvartinden and in the valley ground.

Measurements were ongoing from September 2009 to August 2013 for 10 out of 14 loggers. For R09 and R10 only data for 2009–2011 exists, while R12 and R13 where first installed in 2011, thus yielding data for 2011 to 2013. Nine RST-loggers (type M-Log5W and redesigned UTL-1; identified as R# loggers in text and figures) were installed in vertical rock faces on rock outcrops and along small cliffs with different aspects, while five SST-loggers (standard UTL-1/UTL-3; identified as S# loggers in text and figures) were placed directly into the soil at ca. 10 cm depth, in order to measure SST. One additional logger was placed in a cairn in the valley floor to monitor air temperature. For several of the analyses presented annual mean values were calculated to identify variations in mean annual rock- and soil surface temperature (MARST and MASST respectively) and mean air temperature (MAAT). This ensures easier comparison between the monitoring sites and makes it easier to identify local maxima and minima as well as trends (cf. Isaksen et al., 2011).

2.3 Ground surface temperature modelling

2.3.1. Long-term changes in ground temperatures

To study long-term changes in ground temperatures representative for the same elevation as the failure zone, but for sites with a developed soil cover and where snow accumulates, we used data series from the transient permafrost model CryoGrid2 (CG2; cf. Westermann et al., 2013). The physical basis and operational details of CG2 are documented in Westermann et al. (2013), and only a brief overview over the model properties is given here. CG2 calculates ground temperatures according to Fourier's law of conductive heat transfer in the soil and in the snowpack to determine the evolution of ground temperature over time. Thus, CG2 can deliver the transient response of ground temperatures to a changing climate. In addition to conductive heat transfer, the change of internal energy and temperature in the ground is determined by the latent heat generated/consumed by soil freezing/thawing. Subsurface movement of water is not included and only heat flow in the vertical direction is considered, thus solving an effective 1D problem and neglecting lateral heat flow between neighboring cells. This is justified for grid cell sizes considerably larger than the extent of the vertical modelling domain (cf. Westermann et al., 2013).

The model is forced by operational gridded (1 x 1 km) air temperature (Mohr, 2009; Tveito et al., 2000) and snow-depth (Engeset et al., 2004; Saloranta, 2012). Snow cover data is based on the seNorge snow model (www.senorge.no) that uses gridded observations of daily temperature and precipitation as its input forcing, and simulates, among others, snow water

equivalent (SWE), snow depth (SD), and the snow bulk density (ρ) (Saloranta, 2012). The gridded air temperature for our site is mainly driven by the nearby Skibotn and Rihpojavri weather stations which were validated against our local measurements (see section 3.2). The gridded precipitation for our site is mainly driven by observed precipitation at Skibotn weather station. Since we have no observations of snow cover and owing to the large spatiotemporal variability of snow conditions in our alpine study area, the snow simulations from the seNorge model provide probably the best estimate of the spatial average 1 x 1 km snow conditions for our site (cf., Saloranta, 2012). A grid cell covering Polvartinden and similar in elevation (665 m asl) as the failure zone was selected. In addition a grid cell covering the valley floor was selected for validation against our observations. The model parameters for the lower boundary condition and for ground properties were chosen as in Westermann et al. (2013). The surface geology was based on the major surface sediment classification by the Norwegian Geological Survey (NGU, 2010; Thoresen, 1990). For our study sites and the selected grid cells, the sediment stratigraphy was classified as till and coarse colluvium (class 11 according to the sediment map by NGU, 2010) and followed default settings in CG2 with volumetric fractions of the soil constituents and soil type for each layer as given in Westermann et al. (2013). An interval of snow thermal conductivity (k_{snow}) was regarded as parameter uncertainty by Westermann et al. (2013), and was used as a confining range for the true conditions as a *low* (LC, k_{snow} = 0.3 $Wm^{-1}K^{-1}$) and a *high* (HC, k_{snow} = 0.5 $Wm^{-1}K^{-1}$) conductivity scenario run of CG2. For validation, one year of daily SST data from the CG2-model was compared with observed SST-data from our valley and mountain sites. To study long-term changes in ground temperatures and to avoid dominance of near-surface high-frequency temperature variations we selected 10 m depth as an appropriate depth. For more details on the CG2 model, please refer to Westermann et al. (2013).

2.3.2. Subsurface temperature field

We employed a transient three-dimensional transient heat conduction model to get insights into the general pattern of the present subsurface temperature field of Polvartinden. The applied model is discussed in detail in Noetzli et al. (2007a, b) and Noetzli and Gruber (2009) and is basically a finite element model including Fourier's law and phase change via an apparent heat capacity (cf., Mottaghy and Rath, 2006). Where possible, this three-dimensional transient heat conduction model was fed with local datasets. The geometry of the model was based on a 10 m digital terrain model for the surface topography of the entire mountain and a 1000 m rectangular box for the subsurface mass. Values defining the subsurface properties (heat capacity, thermal conductivity, porosity) were obtained from representative sites nearby (cf. Lilleøren et al., 2012) and assumed to be uniform (cf. Table 1). The geothermal heat flux as the lower boundary condition was set to 60 mW m^{-2} (Slagstad et al., 2009). The upper boundary condition was set as a fixed temperature with annual mean values from the distributed near-surface rock temperatures (MARST). Distributed MARST was calculated based on the aspect dependency of MARST. For this, the fit curve from the first two years of data (2009/10–2010/11, cf. Fig. 12a) was calculated. MARST changes in the steeper parts of the mountain were assumed to have roughly followed changes in mean annual air temperature (MAAT). The regional LIA glacier maximum is suggested to have occurred about 1900–1910 (e.g., Ballantyne, 1990; Bakke and others, 2005). Therefore, the time-dependent simulation was started with a steady state temperature field for the MARST

in 1900, and we assumed a linear MAAT increase of 0.55°C until the end of the simulation (Lilleøren et al., 2012), i.e. the year of the rock fall event. Our results are valid for areas that are assumed not to be influenced by a snow cover, i.e., the steep rock-faces of Polvartinden. The main source of uncertainty for the three-dimensional modelling is related to the extrapolation of the MARST.

2.3.3. Lapse rates

To study the surface offset and local influences on air temperature lapse rates for our RST locations, we studied the inter-annual variability from 2009-2013 in monthly mean lapse rates. In the absence of local air temperature measurements at higher elevation (similar to the rock wall loggers), the monthly lapse rates were calculated based on the nearest mountain weather station located at Rihpojavri (502 m asl, Fig. 1a) and our local air temperature measurement site in Signaldalen valley (65 m asl).

3 Results

3.1 Geomechanical characteristics

Based on the laser scanning results, the volume of the rock avalanche was estimated to be approximately 500 000 m^3. These results confirm earlier estimates suggested during the emergency response work initiated directly after the event NGI (2008).

The depth to the failure surface was found to range from 40 m at the back of the failure zone to 0 m at its toe, with the failure zone being a complex wedge with increasing depth of the plane of failure from the front to the back (Fig. 4). Understanding the principle mechanism behind the failure involves a kinematic evaluation of the failure scarp. The extraction of the orientation of the bedding surface and the orientation of the natural slope ("Pre Failure Surface") are determined directly through measurements using the laser scanning data. The discontinuity ordination data are plotted on a stereonet in Figure 5. The bedding planes have been identified as the failure surface from the terrestrial laser scanning data and from interpretation of the GigaPan photography. The green line in Figure 5 represents the orientation of the natural slope surface, and the green circle represents the corresponding daylight window. The white cone depicts an estimated friction surface of 30°. Poles that are contained outside of the white circle but within the green circle are kinematically unstable and represent potential sliding failure planes (Goodman, 1995). The stereonet demonstrates that the bedding surface orientation is steeper than the estimated friction angle, but shallow enough to daylight with respect to the slope face. The bedding surface meets, therewith, the kinematic requirements of a sliding failure posing a potential rockfall hazard (see e.g., Hasler et al., 2012).

The surficial change of the exposed rock mass between 2011 and 2013 is mapped through the comparison of laser scanning data collected at different points in time. The maximum size of blocks released between 2011 and 2013 range from 1 m^3 to

10 m^3. In summary, the repeated laser scanning measurements between 2009, 2011 and 2013 showed little to no rockfall activity, both within the 2008 failure zone and in the adjacent rock slopes.

3.2 Measured mean annual ground surface temperatures

Measured RST and SST data series for the four-year measurements period were smoothed with a 365-day running mean filter (Fig. 6). There is a slightly higher variability for MAAT than for MARST and MASST (at ca 10 cm depth), but the overall correlation is high. MARST and MASST measured during 2009–2013 are between -1.4°C and +2.2°C, with the highest temperatures recorded in the measurement year April 2011 to March 2012 (Logger R05-E). For the vertical rock face sites, the lowest MARST was recorded at the north-facing site in a 365-days period between September 2009 and September 2010 (Logger R06-N).

The large inter-annual variability found in our temperature measurement series is in congruence with general climate conditions in Troms and is confirmed by measurements in nearby mountain slopes (Farbrot et al., 2013). For the monitoring periods 2009–2013, average, minimum and maximum MAAT at the nearby Skibotn meteorological station (27 km to the NNE from Signaldalen) were 0.0°C, 1.2°C below and 1.5°C above the MAAT for the normal period of 1981–2010, respectively.

During 2010/2011 some of the sites were clearly influenced by a snow cover. (cf. Table 2). Based on an analysis of wind direction, wind speed and total snow accumulation at nearby weather stations (among others Skibotn), we assume this difference in snow cover to be caused by inter-annual differences in prevailing wind direction and preferential snow deposition.

We found a very high correlation between our air temperature measurements in the valley bottom (2009–2013) and air temperature data covering the same period from the nearest two meteorological stations at Skibotn (R^2 = 0.99; Fig. 7a) and Rihpojavri (R^2 = 0.97; Fig. 7b). Furthermore, we found a very high correlation between our local air temperature measurements in the Signaldalen valley floor and the rock wall loggers R05 (R^2 = 0.99; Fig. 7c) and R06 (R^2 = 0.98; Fig. 7d). The temperature series from loggers R05 and R06 were chosen because they seem least influenced by snow and they are also the "warmest" and "coldest" loggers, respectively, in the four-year measurement period. Temperatures at logger site R05 are about 1.3°C higher than at the north-facing series at logger site R06. This good correlation allowed us for using the meteorological data from Skibotn for modelling of the long-term evolution of MARST at R05 and R06 for evaluating the potential permafrost distribution near the original failure zone on Polvartinden and recent RST changes by coupling our in-situ surface temperature data with regional and large-scale climate data.

3.3 Modelled mean annual ground temperatures

In order to be able to link our short temperature rock wall series to the greater regional climate development, we compare it to synthetic series based on the regressions presented in Figure 7 and the CG2 simulations. The CG2 model results are representative for our soil temperature sites in the valley floor and in flatter areas at ca. 665 m asl (which is roughly the altitude of the failure zone), where snow accumulates and where our soil temperature loggers were installed.

A one-year comparison of observed daily SST at sites with an established soil and snow cover and the modelled SST from the CG2 model is shown in Figure 8. As seen in Figure 8a the SST observed in the valley floor is in good agreement (R^2 = 0.86 to 0.88) with the CG2 model results for a grid cell with approximately the same elevation as the valley floor. The Signaldalen valley is dominated by mountain birch forest and is characterized by an open forest layer with heather and lichen species dominating the forest floor layer. This type of forest causes snow to accumulate and insulates the ground against strong cooling (cf. Isaksen et al., 2008; Farbrot et al., 2013), an effect which can be seen in our CG2 model results. In the mountains (Fig. 8b) there is a somewhat weaker correlation (R^2 = 0.69 to 0.82) between observed and modelled data. The MASST are about 1 to 1.5°C lower than in the CG2 model for the corresponding grid cell with similar elevation. The warm bias of the simulations during winter is mainly explained by the different snow conditions assumed in the model: while our observational sites in the mountains are affected by considerably strong snow cover variations induced by wind drift, the snow model used as input in the CG2-model generally overestimates snow depths in high mountain areas (cf. Saloranta, 2012). This is also in line with results of an equilibrium permafrost model used by Gisnås et al. (2013) who found a better agreement between the CG2-model and their validation data when the snow depth in the snow model data was reduced by 30% for areas above the tree line. During summer, on the other hand, our observed SST in the mountains are well reproduced by the CG2 simulations.

The coupling of our coldest in-situ RST data from R06 with the climate data from Skibotn since 1958 (cf. Fig. 7d) suggests that the highest MARST on record was 1.1°C and occurred in the 12-month period between March 2007 and February 2008, i.e., ending four months before the Signaldalen rock avalanche detached (Fig. 9a). A comparison with the CG2 model data run at 10 m depth for the same period suggests a gradual warming and degradation of the permafrost and supports our synthetic series with the warmest period occurring just a few months prior to the failure. Figure 9b shows the recent 10-year period for the synthetic series and the four-year series of the in-situ MARST data for the lowest (R06) and the highest (R05) rock wall temperatures, covering the range of the measured rock wall temperatures. The figure also shows the two CG2 model runs. According to Westermann et al. (2013) the thermal conductivity of the snow is the largest source of uncertainty in CG2, thus a low (LC) and a high conductivity (HC) scenario run of CG2 are used for the last 10 years as a confining range for the true conditions. Note that the synthetic series are slightly warmer than the series for R06 during the first two years.

The deviation is likely to be due to a thin snow cover that partly covered the rock-face/outcrop particularly the second winter of the monitoring campaign.

Since 1958, the CG2 results clearly indicate warming. Coincidentally, the period Apr 2011 to Mar 2012 was as warm as the previous record from the early 1990s. On the other hand, our measurements took place during the coldest period since 1988. Our measurement period covers, in other words, most of the temperature regime that can be expected in this region within a multi-decadal perspective. The depth of the fracture zone varies between 20 to 40 m (Fig. 4). Temperature penetration from the surface to such depths typically takes between one (20 m) to two years (40 m) (cf. e.g., Gruber et al., 2004a). There is, therefore, a good temporal link between the maximum ground temperature at 20-40 m depth (through at least the last 50-60 years) and the actual timing of the rock avalanche release.

The general pattern of the transient 3D-temperature field in the mountain is illustrated with a 2D transection from South to North in Figure 12. The curve of the isotherms inside the mountain stems from the topography and more pronounced the steeper the topography is (Noetzli et al., 2007). Since the difference in MARST is only in the order of 1.5°C, the isotherms are a little inclined towards the colder mountain flank, however, the main temperature change in the subsurface is experienced with a change in altitude (unlike in e.g. very steep peaks in the Alps, where the main temperature chance is experienced with the position between different warm mountain flanks). Based on this schematic sketch of the subsurface temperatures, the permafrost body underlies all of the steeper part of the mountain and is several hundred meters thick at some places. In the area of the rock fall starting zone more shallow permafrost is simulated.

3.4 Local lapse rate

As shown in Figure 7b our regression analysis shows a high correlation between the nearest mountain weather station located at Rihpojavri (502 m asl, Fig. 1) and our local air temperature measurement site in Signaldalen valley (65 m asl, Fig. 3b). Figure 9 reveals an annual median lapse rate of 6.1°C km^{-1}, but with substantial seasonal and inter-annual variability. Lapse rates are smallest (4–6°C km^{-1}) in late-summer to early autumn, and largest (7–10°C km^{-1}) in spring. We see the strongest gradients in spring (May).

The monthly temperature difference (ΔT) between calculated air temperature and measured rock face temperatures are shown in Figure 11. For the sites R03, R04 and R12, periods during which the loggers obviously had been covered by snow (cf. Table 2) were omitted. Monthly values were calculated in the same way as used for the lapse-rate calculations (cf. section 3.4, Fig. 10). The results in Figure 11 show a clear aspect dependency with a slightly lower permafrost limit in northern exposition as opposed to slopes exposed to the South. The figure also shows the year-to-year variations in the order of ±0.5 to 1.0°C. There is a clear seasonal dependency, with ΔT near 0°C or even negative during autumn and early winter, and largest ΔT (1.5 to 5°C) in late spring and early summer.

Figure 12a shows the annual temperature difference (ΔT) between calculated air temperature and measured rock face temperatures and aspect dependency as derived from the data. The points represent the mean values and the black line is the best polynomial fit to the data ($R^2 = 0.84$). The grey lines show the polynomial fit to the interquartile range of ΔT. The ΔT for logger R06, which is the logger facing most towards north (10°), is +0.6°C as compared to air temperature, while the two loggers facing most towards south (R05, 90° and R09, 208°) show both a ΔT of +1.7°C. We, thus, find an aspect difference between north and south facing loggers of 1.1°C. Figure 12b shows the subsurface temperature field as modelled with the stationary three-dimensional transient heat conduction model (Noetzli et al., 2007a, b) based on rock wall temperature data from 2009–2011. The figure shows a slice transecting Polvartinden mountain from South (left) to North (right).

4 Discussion

Many studies related to mountain climate and permafrost research operate with uniform and/or constant lapse rates of 6.0 or 6.55°C km^{-1}, justifying this by these values being the typical theoretical adiabatic lapse rate. However, theoretical adiabatic lapse rate can vary considerably (from 3 to 9°C km^{-1} for surface conditions at mid-latitudes) due to its dependency on pressure and temperature (Minder et al., 2010). In valley bottoms temperature inversions and cold air pooling can affect lapse rates (e.g., Rolland, 2003), and channelled flow over mountain passes can result in large local temperature anomalies (e.g., Steenburgh et al., 1997).

Our study suggest that the high lapse rate values we find in Signaldalen in spring are caused by the fact that the snow cover normally is depleted in the valley bottom in late spring, while the higher areas and the northerly exposed moderately steep mountain slopes still exhibit an extensive snow cover. These results are in accordance with international literature (e.g., Minder et al., 2010) and are likely applicable to other mountainous areas in northern Norway. Other studies have also shown that seasonal cycles in lapse rates have similar amplitudes to those found in our study, but that the phasing of the seasonality varies (Bolstad et al., 1998; Rolland, 2003; Tang and Fang, 2006; Blandford et al., 2008; Gardner et al., 2009). They also highlight the importance of local air temperature measurements in experimental observational networks to reduce uncertainty. Our results clearly support these findings.

Our measured MARST and MASST values from the period 2009–2013 indicate warm/marginal permafrost at all temperature logger sites facing north-northeast, i.e., in the same aspect as the failure zone. Our results yield an estimated mean lower limit of permafrost at around 600-650 m asl; this value is in agreement with earlier estimates in the inner fjord- and valley areas of Troms (Farbrot et al., 2013; Gisnås et al., 2016) and coincides with the upper limit of the failure zone. Since all rock wall loggers are installed at small cliffs (rather than in vertical, large rock walls) the snow close and/or atop these cliffs can attenuate normal winter cooling and, thus, affect the results during the winter months. This is visible in

Figure 11, where some of the NE-facing loggers exhibit a clearly higher winter temperatures than what would be expected when compared with air temperature. The influence of the snow cover on the rock thermal regime has been studied in steep rock walls (Haberkorn et al., 2015a, b; Hasler et al., 2011; Magnin et al., 2015). The highly variable spatial and temporal distribution of the snow cover strongly influences the ground thermal regime of steep rock faces (Haberkorn et al., 2015a, b; Magnin et al., 2015). Haberkorn et al. (2015a) found that snow depths exceeding 0.2 m were enough to have an insulating effect on steep, bare bedrock. Such amounts are likely to accumulate in steep, high rock walls with a certain degree of surface roughness. As snow reduces ground heat loss in winter, it has an overall warming effect on both N- and S-facing rock walls despite the fact that it provides protection from solar radiation in early summer (Haberkorn et al., 2017). However, in moderately inclined (45–70°) sun-exposed rock walls Hasler et al. (2011) suggest a reduction of MARST of up to 3°C compared to estimates in near-vertical, compact rock due to snow persistence during the months with most intense radiation. For our study some of the soil logger sites feature moss or thin vegetation (like the mountainside otherwise) which also affects the temperature. Together, the loggers (including the soil loggers) encompass the variation of the snow and surface conditions present around the Signaldalen rock avalanche site.

The long-term development in the annual mean temperatures from the instrumental period (the late 1800-century) in northern Norway can be split into four periods: a cold period in the beginning, a period referred to as "early 20th century warming" culminating in the 1930s, a period with cooling from the 1930s to the 1960s, and finally the "recent warming" from the 1960s to present (Hanssen-Bauer et al., 2015). Regional climate data since 1958 from Skibotn weather station suggest a general warming of the greater Signaldalen area. This is in agreement with the general atmospheric warming (Hanssen-Bauer et al., 2015) and observed permafrost temperature rise (Isaksen et al., 2007) and the long-term permafrost degradation (Farbrot et al., 2013) in northern-Norway, with an observed peak during the period 2007–2009 (Christiansen et al., 2011; Romanovsky et al., 2016). The CG2 model results suggest (not shown) an increase of the lower permafrost limit for snow covered sites from ca. 600 m asl in the 1960s to about 800 m asl between 2000–2010 (Westermann, personal communication, 2015). Our modelled data (Fig. 9) and observed ground temperature data from the nearby Guolasjávri permafrost borehole (Fig. 13, see location in Fig. 1) suggest that the highest mean near surface temperatures on record occurred in the period between March 2007 and February 2008, thus ending only a few months before the Signaldalen rock avalanche detached.

According to a study by Fischer et al. (2012) on potential triggering factors at 56 historical rock avalanche and rockfall events in the Alps, it seems to be the marginal permafrost zones where most of the recent changes concerning ice content and hydrology have taken place; parameters that are seen as having an important influence on slope stability also by, e.g., Allen and Huggel (2013), Deline et al. (2011) and Fischer et al. (2013). In laboratory studies, Davies et al. (2001) demonstrated that the shear strength of an ice-bonded rock discontinuity significantly reduces with warming and that the minimum shear stress is reached between ca. -0.5 and 0°C. Krautblatter et al. (2013) showed that fracture ice influences stability down to a

depth of approximately 20 m, below that depth, the overburden pressure of the rock mass is becoming too high. According to their study, intact rock bridges and rock-rock-contacts exert additional control on rock stability. While permafrost increases the uniaxial and tensile strength of such rock bridges and rock-rock-contacts, warming of permafrost decreases these strengths and could, thus, trigger rock slope failures. In degrading permafrost, rock-mechanical properties may control early stages of destabilization and become more important for higher normal stress, i.e. higher magnitudes of rock slope failure. Ice-mechanical properties outbalance the importance of rock-mechanical components after the deformation accelerates and are more relevant for smaller magnitudes (Krautblatter et al., 2013). In early summer, the combined effect of hydrostatic and cryostatic pressure can cause a peak in shear force exceeding high frozen shear resistance (Draebing et al., 2014).

Analysing temperature conditions prior to 144 past rockfall events in the Swiss Alps and the French Mont Blanc massive, Lüthi et al. (2015) recently showed that small to medium-sized rockfalls (with volumes up to 100'000 m^3) mainly occurred during short-term periods of unusually high temperatures, whereas larger high-elevation rock slope failures occur all year-round. Hasler et al. (2011) showed that local warming of cold permafrost may be induced by advection and the related erosion of cleft ice, and that permafrost degradation through thermal advection by running water can rapidly lead to the development of deep thaw corridors along fracture zones and potentially destabilise much larger volumes of rock than through thermal conduction on similar timescales. Draebing et al. (2016) found that the rock mechanical regime also was snow-controlled in permafrost rock slopes at Steintaelli in the Swiss Alps. They found that during snow-free periods, high-frequency thermal expansion and contraction occurred. Rock temperature locally dropped to -10°C, resulting in thermal contraction of the rock slopes. Snow cover insulation maintained temperatures in the frost-cracking window and favoured ice segregation. Such repetitive occurrence destabilises the rock slope and can potentially lead to failure (Draebing et al., 2016).

A recent synopsis of MARST at 34 locations within the PERMOS network in Switzerland (PERMOS, 2016) shows that MARST are generally higher than MAAT. In south-exposed near-vertical locations this difference amounts to up to 10°C, in north exposed locations MARST is only slightly higher than MAAT (PERMOS, 2016). Similar values were also measured in steep alpine rock walls at the Matterhorn and the Jungfraujoch in Switzerland (by Hasler et al., 2011) and at the Aiguille du Midi in France (by Magnin et al., 2015). In Scandinavia, the amount of studies using direct observations to explore the influence of solar radiation on near surface temperatures in different aspects of steep mountain walls is limited so far. In Jotunheimen in southern Norway north-facing rock wall surfaces were on average less than 1°C warmer than the surrounding air temperature, while MARST in more radiation exposed rock walls was up to 4°C higher than MAAT (Hipp et al., 2014). Generally, the influence of direct solar radiation is less pronounced at high latitudes than in mid-latitude mountains. Our results indicate an altitudinal difference of roughly 200–250 m between northerly and southerly aspect (cf. Fig. 12b), as compared to 1000–1500 meters (or up to 8–10 °C) for some sites in the Swiss Alps (PERMOS, 2016). Due to our small sample size these results should be seen as tentative estimates. Also, the potential effect of the midnight sun has not been looked at. In addition, it has to be noted that we lack loggers exposed directly to the South. Based on the shape of

the polynomial fit curve (Fig. 12a), and on what is known from other studies (e.g., Gruber et al., 2004a; Noetzli and Gruber, 2009; Magnin et al., 2015; PERMOS, 2016), the difference between northerly and southerly aspects is probably 0.2 to 0.4°C higher than indicated by our measurements. This would yield an absolute difference between "warmest" and "coldest" aspects of approximately 1.3 to 1.5°C, which still is considerably lower than for mid-latitude mountain ranges and about 1.5°C lower that were reported by Hipp et al. (2014) for a location in southern Norway, thus supporting strongly decreasing aspect dependency with increasing latitude. Smaller differences in MARST between North and South-facing rock walls eventually result in less pronounced 3D effects of the subsurface temperature field as illustrated with the modelling results of the subsurface temperature field (Fig. 12b). For alpine peaks with a triangular geometry, isotherms can be nearly vertical in the uppermost part of mountain peaks in the European Alps (cf. Noetzli et al., 2007b) and temperatures change mainly with the position between North and South-facing slopes. Here, isotherms are only little inclined, and the main change in subsurface temperatures is experienced with changing altitude and not changing exposition.

5 Conclusions

Analyses based on four-year rock- and soil surface temperature series suggest warm/marginal permafrost at several of the investigated sites in Signaldalen, and yield an estimated mean lower limit of permafrost at around 600-650 m asl, an altitude which coincides with the upper limit of the failure zone. Regional climate data since 1958 and nearby borehole data suggest a general warming and that the highest mean near surface temperatures on record occurred some months before the Signaldalen rock avalanche detached. These findings are supported by model results of the transient permafrost model CG2. Our results give also new insights into aspect dependency of mountain permafrost in northern Scandinavia, a subject that so far has been little explored. We found an absolute difference in ground surface temperatures of approximately 1.3 to 1.5°C between south- and north exposed slopes.

The volume calculation based on terrestrial laser scanning data show that the depth to the actual failure surface was found to range from 40 m at the back to 0 m at the toe. The repeated laser scanning between 2009 and 2013 show little to no activity in both the 2008 failure zone and the adjacent rock slopes. Considering that temperature penetration to, e.g., 15–20 m depth in frozen rock typically takes one year it is likely that changing rock-/ice-temperatures due to the general warming and in response to the extreme warm previous year have played an important role in the detaching of the Signaldalen rock avalanche.

Acknowledgements

The work of Regula Frauenfelder was funded by the Norwegian Research Council (through its base funding to NGI), the work of Ketil Isaksen was funded through the Norwegian Meteorological Institute, all this funding is greatly acknowledged.

We are indebted to Leif Skogli (Signaldalen) who let us install loggers on his property and helped with the logistics during the laser scanning campaigns. We would also like to thank Steinar Engsted (former employee at Storfjord municipality) for his interest in our work. Kjetil Brattlien (NGI), Gunnar Kristensen (NVE) and Gunilla Kaiser are thanked for letting us use their imagery. Herman Farbrot, Gunilla Kaiser and Kristin Sæterdal Myhra are acknowledged for their help in the field. Last but certainly not least, Sebastian Westermann (UiO) deserves a great thanks for running his CG2 model for us and letting us use the according results.

References

Allen, S. K., Cox, S. C., and Owens, I. F.: Rock avalanches and other landslides in the central Southern Alps of New Zealand: a regional study considering possible climate change impacts, Landslides, 8, 33–48, doi:10.1007/s10346-010-0222-z, 2011.

Allen, S. and Huggel, C.: Extremely warm temperatures as a potential cause of recent high mountain rockfall, Global and planetary change, 107 (2013), 59-69, 2013.

Auer, I., Böhm, R., Jurkovic, A., Lipa, W., Orlik, A., Potzmann, R., Schöner, W., Ungersböck, M., Matulla, C., Briffa, K., Jones, P., Efthymiadis, D., Brunett,i M., Nanni, T., Maugeri, M., Mercalli, L., Mestre, O., Moisselin, J-M., Begert, M., Müller-Westermeier, G., Kveton, V., Bochnicek, O., Stastny, P., Lapin, M., Szalai, S., Szentimrey, T., Cegnar, T., Dolinar, M., Gajic-Capka, M., Zaninovic, K., Majstorovic, Z., and Nieplova, E.: HISTALP - Historical instrumental climatological surface time series of the Greater Alpine Region. Int J Climatol 27(1):17–46, 2007.

Ballantyne, C.K.: The Holocene glacial history of Lyngshalvøya, northern Norway- chronology and climatic implications., Boreas ,19 (2), 93–117, 1990.

Bakke, J., Dahl, S.O., Paasche, O., Lovlie, R., and Nesje, A.: Glacier fluctuations, equilibrium-line altitudes and palaeoclimate in Lyngen, northern Norway, during the Lateglacial and Holocene, The Holocene, 15 (4), 518–540, 2005.

Barla, G., Dutto, F., and Mortara, G.: Brenva Glacier rock avalanche of 18 January 1997 on the Mont Blanc range, northwest Italy, Landslide News, 13, 2–5, 2000.

Blandford, T. R., Humes, K. S., Harshburger, B. J., Moore, B. C., Walden, V. P. and Ye, H.: Seasonal and Synoptic Variations in Near-Surface Air Temperature Lapse Rates in a Mountainous Basin, Journal of Applied Meteorology and Climatology, 47(1), 249–261, doi:10.1175/2007JAMC1565.1, 2008.

Blikra, L. H. and Christiansen, H. H.: A field-based model of permafrost-controlled rockslide deformation in northern Norway, Geomorphology, 208, 34–49, doi:10.1016/j.geomorph.2013.11.014, 2014.

Blikra, L. H., Christensen, H. H., Kristensen, L., and Lovisolo M.: Characterization, Geometry, Temporal Evolution and Controlling Mechanisms of the Jettan Rock-Slide, Northern Norway, Engineering Geology for Society and Territory-Volume 2. Springer International Publishing, 273-278, 2015.

Blikra, L. H., Longva, O., Braathen, A., Anda, E., Dehls, J. F., Stalsberg, K.: Rock slope failures in Norwegian fjord areas; examples, spatial distribution and temporal pattern, Landslides From Massive Rock Slope Failure, Springer Dordrecht, The Netherlands, 475–496, 2006.

Bolstad, P. V., Swift, L., Collins, F. and Régnière, J.: Measured and predicted air temperatures at basin to regional scales in the southern Appalachian mountains, Agricultural and Forest Meteorology, 91(3–4), 161–176, doi:10.1016/S0168-1923(98)00076-8, 1998.

Brunetti, M., Lentini, G., Maugeri, M., Nanni, T., Auer, I., Böhm, R., and Schöner, W.: Climate variability and change in the Greater Alpine Region over the last two centuries based on multivariable analysis. Int J Climatol 29(15), 2197–2225, 2009.

Christiansen, H. H., Etzelmüller, B., Isaksen, K., Juliussen, H., Farbrot, H., Humlum, O., Johansson, M., Ingeman-Nielsen, T., Kristensen, L., Hjort, J., Holmlund, P., Sannel, A. B. K., Sigsgaard, C., Åkerman, H. J., Foged, N., Blikra, L. H., Pernosky, M. A., and Ødegård, R..: The Thermal State of Permafrost in the Nordic area during the IPY 2007-2009, Permafrost and Periglacial Processes 21, 156–181, DOI: 10.1002/ppp.687, 2010.

Cola, G.: The large landslide of the south-east face of Thurwieser peak (Thurwieser-Spitze) 3658 m (Upper Valtellina, Italy), Terra Glacialis, 8, 38–45, 2005.

Crosta, G. B., Chen, H., and Lee, C. F.: Replay of the 1987 Val Pola Landslide, Italian Alps, Geomorphology, 60, 127–146, 2004.

Davies, M. C. R., Hamza, O., and Harris, C.: The effect of rise in mean annual temperature on the stability of rock slopes containing ice-filled discontinuities, Permafrost Periglac. Process., 12, 137–144. doi:10.1002/ppp.378, 2001.

Deline, P., Alberto, W., Broccolato, M., Hungr, O., Noetzli, J., Ravanel, L., and Tamburini, A.: The December 2008 Crammont rock avalanche, Mont Blanc massif area, Italy, Nat. Hazards Earth Syst. Sci., 11, 3307–3318, doi:10.5194/nhess-11-3307-2011, 2011.

Draebing, D., Krautblatter, M., Dikau, R.: Interaction of thermal and mechanical processes in steep permafrost rock walls: A conceptual approach, Geomorphology 226, 226–235. DOI:10.1016/j.geomorph.2014.08.009, 2014.

Draebing, D., Haberkorn, A., Krautblatter, M., Kenner, R., Phillips, M.: Thermal and Mechanical Responses Resulting From Spatial and Temporal Snow Cover Variability in Permafrost Rock Slopes, Steintaelli, Swiss Alps, Permafrost and Periglac. Process., DOI:10.1002/ppp.1921, 2016.

Engeset, R., Tveito, O. E., Alfnes, E., Mengistu, Z., Udnæs, H.-C., Isaksen, K., and Førland, E. J.: Snow map system for Norway, 23rd Nordic Hydrological Conference, Tallin, Estonia. NHP Report 48, 112–121, 2004.

Etzelmüller, B., Berthling, I. and Sollid, J. L.: Aspects and concepts on the geomorphological significance of Holocene permafrost in southern Norway, Geomorphology, 52(1–2), 87–104, doi:http://dx.doi.org/10.1016/S0169-555X(02)00250-7, 2003.

Evans, S. G. and Clague, J. J.: Recent climatic change and catastrophic geomorphic processes in mountain environments, Geomorphology, 10, 107–128, 1994.

Farbrot, H., Isaksen, K., and Etzelmüller, B.: Present and past distribution of mountain permafrost in the Gaissane Mountains, northern Norway, Proceedings of the Ninth International Conference on Permafrost, Kane, D. L., Hinkel, K. M. (eds), Institute of Northern Engineering, University of Alaska Fairbanks, Fairbanks, Alaska, USA, 427–432, 2008.

Farbrot, H., Isaksen, K., Etzelmüller, B., and Gisnås, K.: Ground Thermal Regime and Permafrost Distribution under a Changing Climate in Northern Norway, Permafrost and Periglacial Processes, DOI: 10.1002/ppp.1763, 2013.

Fischer, L., Purves, R.S., Huggel, C., Noetzli, J. and Haeberli, W.: On the influence of topographic, geological and cryospheric factors on rock avalanches and rockfalls in high-mountain areas, Natural Hazards and Earth System Sciences 12, 241–254, 2012.

Fischer, L., Huggel, C., Kääb, A., and Haeberli, W.: Slope failures and erosion rates on a glacierized high-mountain face under climatic changes, Earth surface processes and landforms, 38 (8), 836-846, 2013.

Frauenfelder, R., Isaksen, K., Noetzli, J., Lato, M. J., Smebye, H. C.: Analysing ground temperatures and geomechanical mapping of the 2008 Signaldalen rock slide. A case study from Northern Norway, Extended abstract 6th Canadian GeoHazards Conference - GeoHazards 6, 2014.

Gardner, A. S., Sharp, M. J., Koerner, R. M., Labine, C., Boon, S., Marshall, S. J., Burgess, D. O. and Lewis, D.: Near-Surface Temperature Lapse Rates over Arctic Glaciers and Their Implications for Temperature Downscaling, Journal of Climate, 22(16), 4281–4298, doi:10.1175/2009JCLI2845.1, 2009.

Geertsema, M., Clague, J. J, Schwab, J. W., and Evans, S. G.: An overview of recent large catastrophic landslides in northern British Columbia, Canada, Eng. Geol., 83, 120–143, 2006.

Gisnås, K., Etzelmüller, B., Farbrot, H., Schuler, T., and Westermann, S.: CryoGRID 1.0: Permafrost distribution in Norway estimated by a spatial numerical model, Permafrost Periglac., 24, 2–19, 2013.

Gisnås, K., Etzelmüller, B., Lussana, C., Hjort, J., Sannell, A. B. K., Isaksen, K., Westermann, S., Kuhry, P., Christiansen, H. H.: Permafrost map for Norway, Sweden and Finland, accepted for publication in Permafrost and Periglacial Processes, 2016.

Gobiet, A., Kotlarski, S., Beniston, M., Heinrich, G., Rajczak, J., Stoffel, M.: 21st century climate changes in the European Alps – A review, Science of The Total Environment, 493, 1138–1151, 2014.

Goodman, R.E. Block theory and its application. Geotechnique 45:3, 383-423, 1995

Gruber, S., Hoelzle, M., and Haeberli, W.: Permafrost thaw and destabilization of Alpine rock walls in the hot summer of 2003, Geophys. Res. Lett., 31, L13504, doi:10.1029/2004GL020051, 2004a.

Gruber, S., Hoelzle, M., and Haeberli, W.: Rock wall temperatures in the Alps – modelling their topographic distribution and regional differences, Permafrost and Periglacial Processes 15(3): 299–307, 2004b.

Gruber, S., Peter, M., Hoelzle, M., Woodhatch, I., and Haeberli, W.: Surface temperatures in steep Alpine rock faces - a strategy for regional-scale measurement and modelling, *Proceedings of the 8th International Conference on Permafrost 2003*, Zurich, Switzerland, 325–330, 2003.

Haberkorn, A., Hoelzle, M., Phillips, M., and Kenner, R.: Snow as driving factor of rock surface temperatures in steep rough rock walls, Cold Reg. Sci. Technol., 118, 64–75, doi:10.1016/j.coldregions.2015.06.013, 2015a.

Haberkorn, A., Phillips, M., Kenner, R., Rhyner, H., Bavay, M., Galos, S. P., and Hoelzle, M.: Thermal Regime of Rock and its Relation to Snow Cover in Steep Alpine Rock Walls: Gemsstock, Central Swiss Alps, Geogr. Ann. A, 97, 579–597, doi:10.1111/geoa.12101, 2015b.

Haberkorn, A., Wever, N., Hoelzle, M., Phillips, M., Kenner, R., Bavay, M., and Lehning, M.: Distributed snow and rock temperature modelling in steep rock walls using Alpine3D, The Cryosphere, 11, 585-607, doi:10.5194/tc-11-585-2017, 2017.

Haeberli, W., Hölzle, M., Paul, F., and Zemp, M.: Integrated monitoring of mountain glaciers as key indicators of global climate change: the European Alps. Ann Glaciol 46:150–160, 2007.

Haeberli, W. and Gruber, S.: Gobal warming and mountain permafrost, in Margesin, R. (ed.), Permafrost soils. Berlin, Springer, 205–218, 2009.

Haeberli, W., Noetzli, J., Arenson, L., Delaloye, R., Gärtner-Roer, I., Gruber, S., Isaksen, K., Kneisel, C., Krautblatter, M., Phillips, M.: Mountain permafrost: development and challenges of a young research field, Journal of Glaciology 56 (200), 1043-1058, 2010.

Haeberli, W., Huggel, C., Kääb, A., Polkvoj, A., Zotikov I., and Osokin, N.: The Kolka-Karmadon rock/ice slide of 20 September 2002: An extraordinary event of historical dimensions in North Ossetia, Russian Caucasus, J. Glaciol., 50, 533–546, 2004.

Hanssen-Bauer, I., Førland, E. J., Haddeland, I., Hisdal, H., Mayer, S., Nesje, A., Nilsen, J. E. Ø., Sandven, S., Sandø, A.B., Sorteberg, A., Ådlandsvik, B. (Eds): Klima i Norge 2100 – Kunnskapsgrunnlag for klimatilpasning oppdatert i 2015, NCCS report no. 2/2015, https://klimaservicesenter.no/ (in Norwegian), 2015.

Harris, C. and 21 others: Permafrost and climate in Europe: Monitoring and modelling thermal, geomorphological and geotechnical responses, Earth-Science Reviews 92(3-4), 117-171, 2009.

Hasler, A., Gruber, S., and Haeberli, W.: Temperature variability and offset in steep alpine rock and ice faces, The Cryosphere, 5, 977-988, doi:10.5194/tc-5-977-2011, 2011.

Hasler, A., Gruber, S., and Beutel, J.: Kinematics of steep bedrock permafrost, Journal of Geophysical Research 117: F01016, doi:10.1029/2011JF00 1981, 2012.

Hipp, T. F., Etzelmüller, B., Westermann, S.: Permafrost in Alpine Rock Faces from Jotunheimen and Hurrungane, Southern Norway, Permafrost and Periglacial Processes, doi: 10.1002/ppp.1799, 2014.

Huggel, C., Salzmann, N., Allen, S., Caplan-Auerbach, J., Fischer, L., Haeberli, W., Larsen, C., Schneider, D., and Wessels, R.: Recent and future warm extreme events and high-mountain slope stability, Philosophical Transactions of the Royal Society of London A: Mathematical, Physical and Engineering Sciences 368.1919, 2435-2459, 2010.

Hungr, O., Leroueil, S., and Picarelli, L.: The Varnes classification of landslide types, an update, Landslides, 11(2), 167-194, doi:10.1007/s10346-013-0436-y, 2014.

Isaksen, K., Sollid, J. L., Holmlund, P., and Harris, C.: Recent warming of mountain permafrost in Svalbard and Scandinavia, Journal of Geophysical Research 112, F02S04, doi:10.1029/2006JF000522, 2007.

Isaksen, K., Farbrot, H., Blikra, L. H. Johansen, B., and Sollid, J. L.: Five-year ground surface temperature measurements in Finnmark, northern Norway, Proceedings of the Ninth International Conference on Permafrost, Kane, D. L., Hinkel, K. M. (eds), Institute of Northern Engineering, University of Alaska Fairbanks, Fairbanks, Alaska, USA, 789–794, 2008.

Isaksen, K., Ødegård, R.S., Etzelmüller, B., Hilbich, C., Hauck, C., Farbrot, H., Eiken, T., Hygen, H. O., and Hipp, T. F.: Degrading mountain permafrost in southern Norway: Spatial and temporal variability of mean ground temperatures, 1999-2009, Permafrost and Periglacial Processes. doi: 10.1002/ppp.728, 2011.

Jin, H., Li, S., Cheng, G., Wang, S., and Li, X.: Permafrost and climatic change in China, Global Planet. Change, 26(4), 387–404, 2000.

Juliussen, H., Christiansen, H. H., Strand, G. S., Iversen, S., Midttømme, K., Rønning, J.S.: NORPERM, the Norwegian Permafrost Database–a TSP NORWAY IPY legacy, Earth System Science Data, 2, 235-246, doi:10.5194/essd-2-235-2010, 2010.

Krautblatter, M., Funk, D., Günzel, F.K.: Why permafrost rocks become unstable: a rock–ice-mechanical model in time and space, Earth Surface Processes and Landforms, 38, 876–887. DOI:10.1002/esp.3374, 2013.

King, L.: Zonation and Ecology of High Mountain Permafrost in Scandinavia, Geografiska Annaler. Series A, Physical Geography, 68(3), 131, doi:10.2307/521452, 1986.

Lato M., Hutchinson D.J., Gauthier D., Edwards T., Ondercin M.: Comparison of ALS, TLS and terrestrial photogrammetry for mapping differential slope change in mountainous terrain. Canadian Geotechnical Journal, 10.1139/cgj-2014-0051, 2014.

Lato M, Diederichs M, and Hutchinson D.J. Bias correction for static LiDAR scanning of rock outcrops for structural characterization. Rock Mechanics and Rock Engineering, 43 (5), 615-628. 2010.

Lato M, Diederichs M.S, Hutchinson D.J, Harrap R. Evaluating roadside rockmasses for rockfall hazards using LiDAR data: optimizing data collection and processing protocols. Nat. Hazards. Vol. 60(2) pp. 831-864. 2012.

Lilleøren, K., Etzelmüller, B., Gisnås, K., Humlum, O.: The relative age of mountain permafrost-estimation of Holocene permafrost limits in Norway, Global and Planetary Change, 92, 2012.

Luethi, R., Gruber, S., Ravanel, L.: Modelling transient ground surface temperatures of past rockfall events: towards a better understanding of failure mechanisms in changing periglacial environments, Geografiska Annaler: Series A, Physical Geography, xx, 1–15, DOI:10.1111/geoa.12114, 2015.

Magnin, F., Deline, P., Ravanel, L., Noetzli, J., and Pogliotti, P.: Thermal characteristics of permafrost in the steep alpine rock walls of the Aiguille du Midi (Mont Blanc Massif, 3842 m a.s.l), The Cryosphere, 9, 109-121, doi:10.5194/tc-9-109-2015, 2015.

Marchenko, S. S., Gorbunov, A. P., and Romanovsky, V. E.: Permafrost warming in the Tien Shan mountains, Central Asia, Global Planet. Change, 56(3–4), 311–327, 2007.

Minder, J. R., Mote, P. W., and Lundquist, J. D.: Surface temperature lapse rates over complex terrain: Lessons from the Cascade Mountains, Journal of Geophysical Research, 115(D14), doi:10.1029/2009JD013493, 2010.

Mohr, M.: Comparison of versions 1.1 and 1.0 of gridded temperature and precipitation data for Norway. met.no note 19/2009 (http://met.no/filestore/note19-09.pdf), 2009.

Mottaghy, D. and Rath, V.: Latent heat effects in subsurface heat transport modelling and their impact on palaeotemperature reconstructions, Geophysical Journal International, 164, 236–245, doi:10.1111/j.1365-246x.2005.02843.x, 2006.

Myhra, K. S., Westermann, S., and Etzelmüller, B.: Modelled Distribution and Temporal Evolution of Permafrost in Steep Rock Walls Along a Latitudinal Transect in Norway by CryoGrid 2D, *Permafrost and Periglacial Processes*, doi:10.1002/ppp.1884, 2015.

NGU: Produktspesifikasjon ND Løsmasser, Norges Geologiske Undersøkelser, 37/99, 2010. (In Norwegian)

Noetzli, J., Gruber, S., Kohl, T., Salzmann, N., and Haeberli, W.: Three-dimensional distribution and evolution of permafrost temperatures in idealized high-mountain topography, Journal of Geophysical Research: Earth Surface, 112, 2007.

Noetzli, J., and Gruber, S.: Transient thermal effects in Alpine permafrost, The Cryosphere, 3: 85-99, 2009.

Oppikofer, T., Jaboyedoff, M., and Keusen, H.-R.: Collapse at the eastern Eiger flank in the Swiss Alps, Nat. Geosci., 1, 31–535, 2008.

Ødegård, R. S., Hoelzle, M., Vedel Johansen, K. and L. Sollid, J.: Permafrost mapping and prospecting in southern Norway, Norsk Geografisk Tidsskrift - Norwegian Journal of Geography, 50(1), 41–53, doi:10.1080/00291959608552351, 1996.

PERMOS. Permafrost in Switzerland 2010/2011 to 2013/2014, Noetzli, J., Luethi, R., and Staub, B. (eds.), Glaciological Report (Permafrost) No. 12-15 of the Cryospheric Commission of the Swiss Academy of Sciences, 85 pp, 2016.

Phillips, M., Wolter, A., Lüthi, R., Amann, F., Kenner, R., Bühler, Y.: Rock slope failure in a recently deglaciated permafrost rock wall at Piz Kesch (Eastern Swiss Alps), February 2014, Earth Surface Processes and Landforms, doi: 10.1002/esp.3992, 2016.

Ravanel, L. and Deline, P.: Climate influence on rockfalls in high-Alpine steep rockwalls: the north side of the Aiguilles de Chamonix (Mont Blanc massif) since the end of the Little Ice Age, Holocene, 21, 357–365, doi:10.1177/0959683610374887, 2010.

Rolland, C.: Spatial and Seasonal Variations of Air Temperature Lapse Rates in Alpine Regions, Journal of Climate, 16(7), 1032–1046, doi:10.1175/1520-0442(2003)016<1032:SASVOA>2.0.CO;2, 2003.

Romanovsky, V. E., Smith, S. L., Isaksen, K., Shiklomanov, N. I., Streletskiy, D. A., Kholodov, A. L., Christiansen, H. H., Drozdov, D. S., Malkova, G. V., Marchenko, S. S.: Terrestrial permafrost, in "State of the Climate in 2015", Bulletin of the American Meteorological Society, 97 (8), S149–S152, 2016.

Saloranta, T. M.: Simulating snow maps for Norway: description and statistical evaluation of the seNorge snow model, The Cryosphere, 6, 1323-1337, doi:10.5194/tc-6-1323-2012, 2012.

Slagstad, T., Balling, N., Elvebakk, H., Midttømme, K., Olesen, O., Olsen, L., and Pascal, C.: Heat-flow measurements in Late Palaeoproterozoic to Permian geological provinces in south and central Norway and a new heat-flow map of Fennoscandia and the Norwegian–Greenland Sea, Tectonophysics, 473 (3–4), 341–361, 2009.

Steenburgh, W. J., Mass, C. F. and Ferguson, S. A.: The Influence of Terrain-Induced Circulations on Wintertime Temperature and Snow Level in the Washington Cascades, Weather and Forecasting, 12(2), 208–227, doi:10.1175/1520-0434(1997)012<0208:TIOTIC>2.0.CO;2, 1997.

Stoffel, M., Tiranti, D., and Huggel, C.: Climate change impacts on mass movements - case studies from the European Alps, Science of the Total Environment, 493 (2014): 1255-1266, 2014.

Stoffel, M. and Huggel, C.: Mass Movements in Periglacial Environments, in International Encyclopedia of Geography: People, the Earth, Environment and Technology, edited by D. Richardson, N. Castree, M. F. Goodchild, A. Kobayashi, W. Liu, and R. A. Marston, pp. 1–8, John Wiley & Sons, Ltd, Oxford, UK. [online] Available from: http://doi.wiley.com/10.1002/9781118786352.wbieg0815 (Accessed 22 June 2017), 2017.

Tang, Z. and Fang, J.: Temperature variation along the northern and southern slopes of Mt. Taibai, China, Agricultural and Forest Meteorology, 139(3–4), 200–207, doi:10.1016/j.agrformet.2006.07.001, 2006.

Thoresen, M.: Kvartærgeologisk kart over Norge, tema jordarter, Norwegian Geological Survey, Trondheim, Norge, 1990. (In Norwegian).

Tveito, O. E., Førland, E. J., Heino, R., Hanssen- Bauer, I., Alexandersson, H., Dahlstrøm, B., Drebs, A., Kern-Hansen, C., Vaarby Laursen, E., and Westman, Y.: Nordic temperature maps, Report no. 09/00 (http://met.no/filestore/09_00.pdf), DNMI, Oslo, 2000.

Vavrus, S.: The role of terrestrial snow cover in the climate system, Clim. Dyn., 29, 73–88, doi:10.1007/s00382-007-0226-0, 2007.

Wang, Q., Fan, X., and Wang, M.: Recent warming amplification over high elevation regions across the globe, Climate Dynamics, 43, 87-101, doi:10.1007/s00382-013-1889-3, 2014.

Westermann, S., Schuler, T. V., Gisnås, K., and Etzelmüller, B.: Transient thermal modeling of permafrost conditions in Southern Norway, The Cryosphere, 7(2), 719–739, doi:10.5194/tc-7-719-2013, 2013.

Table and Figures

Table 1. Values for subsurface properties as used in the stationary three-dimensional transient heat conduction modelling**.**

Subsurface property	Value (Value range)
Heat capacity	850 J kg^{-1} K^{-1}
Thermal conductivity	2-2.5 Wm^{-1} K^{-1}
Density	2800-2900 kg m^{-3}
Water content	0.2-1 %

Table 2. Rock wall and soil temperature loggers installed in Polvartinden and Signaldalen. Snow cover = estimated winter snow cover based on a simple evaluation of day-to-day temperature variability and standard deviation compared to reference logger R05, divided into three categories: I) snow cover mostly absent, II) snow cover over short periods, III) snow cover over longer periods.

Site	Elevation (m asl)	Aspect (°)	Snow cover
A01-SD	65	-	-
R03-NE	640	30	III
R04-NW	657	290	III
R05-E	630	90	I
R06-N	632	10	I-II
R09-SW	646	208	I
R10-NE	598	40	I
R12-NE	668	45	II-III
R14-NNE	608	35	II
S02-SD	64	-	III
S02	664	-	I-II
S07	626	-	II
S08	648	-	I-II
S11	540	-	II
S13	643	-	III

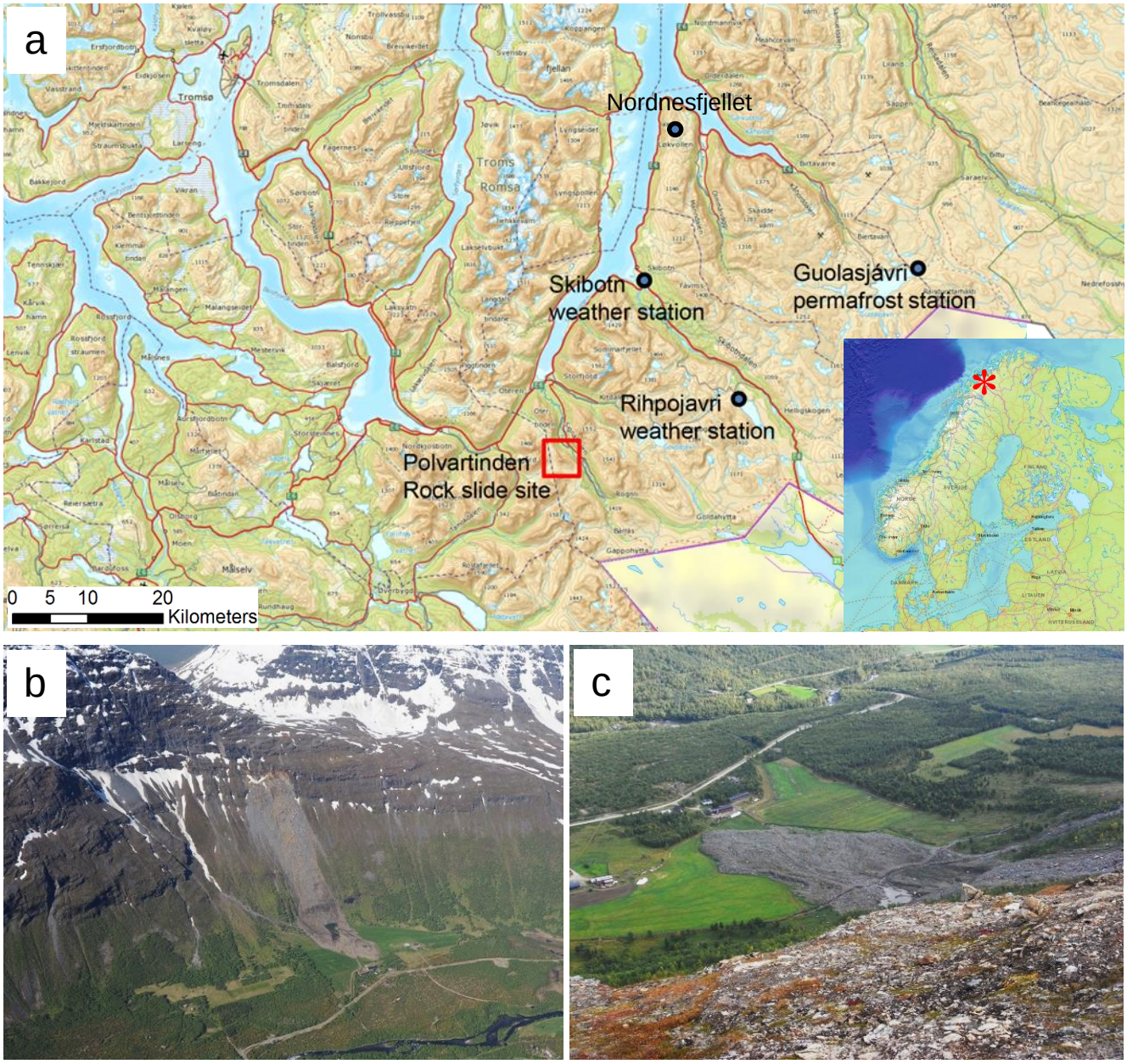

Figure 1. a) Key map showing the location of the Polvartinden rock avalanche site, the two weather stations and the permafrost station used in this study (map source: Copyright © by Norwegian Mapping Authority/Statens kartverk); b) Signaldalen rock avalanche as seen from helicopter on 28.7.2009 (Photograph by courtesy of Gunnar Kristiansen, NVE); c) runout area of the Signaldalen rock avalanche in September 2011 (Photograph by courtesy of Gunilla Kaiser).

Figure 2. Visible in-situ ice (encircled areas) observed in the rock avalanche failure zone on June 26th, 2008. The photograph was taken a few hours after the event (Photograph by courtesy of Kjetil Brattlien, NGI).

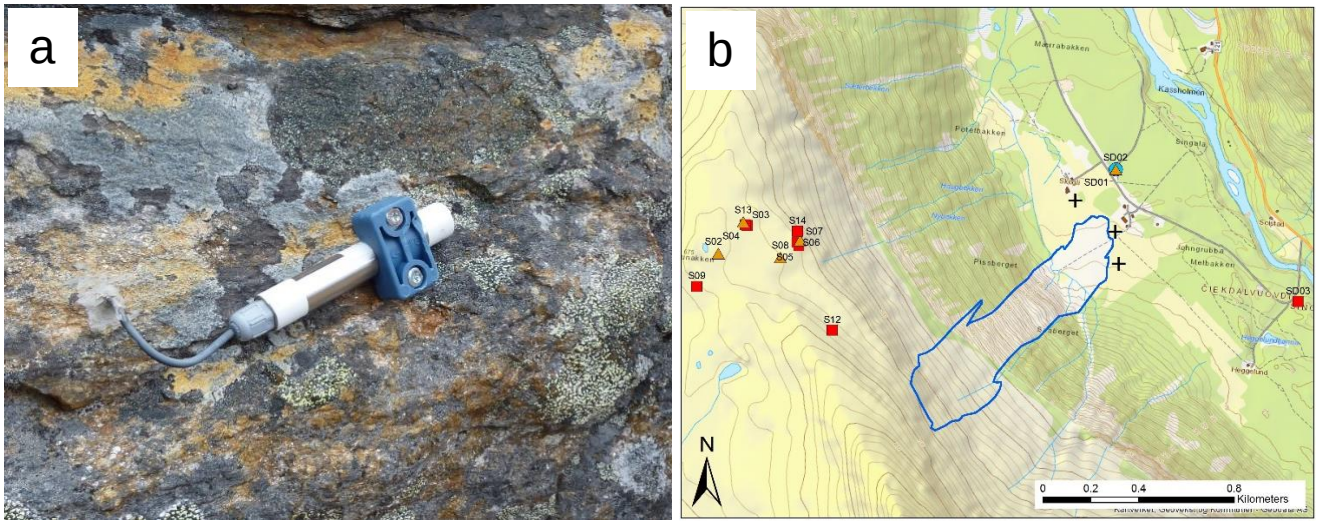

Figure 3. a) Typical logger installation setup; b) Map showing temperature measurement locations in vertical rock faces (red squares), within soil material (yellow triangles) and within a stone cairn (one blue circle in the valley bottom), the three black crosses mark the laser scanning locations. Rock avalanche outline in blue. Map source: Copyright © by Norwegian Mapping Authority/Statens kartverk.

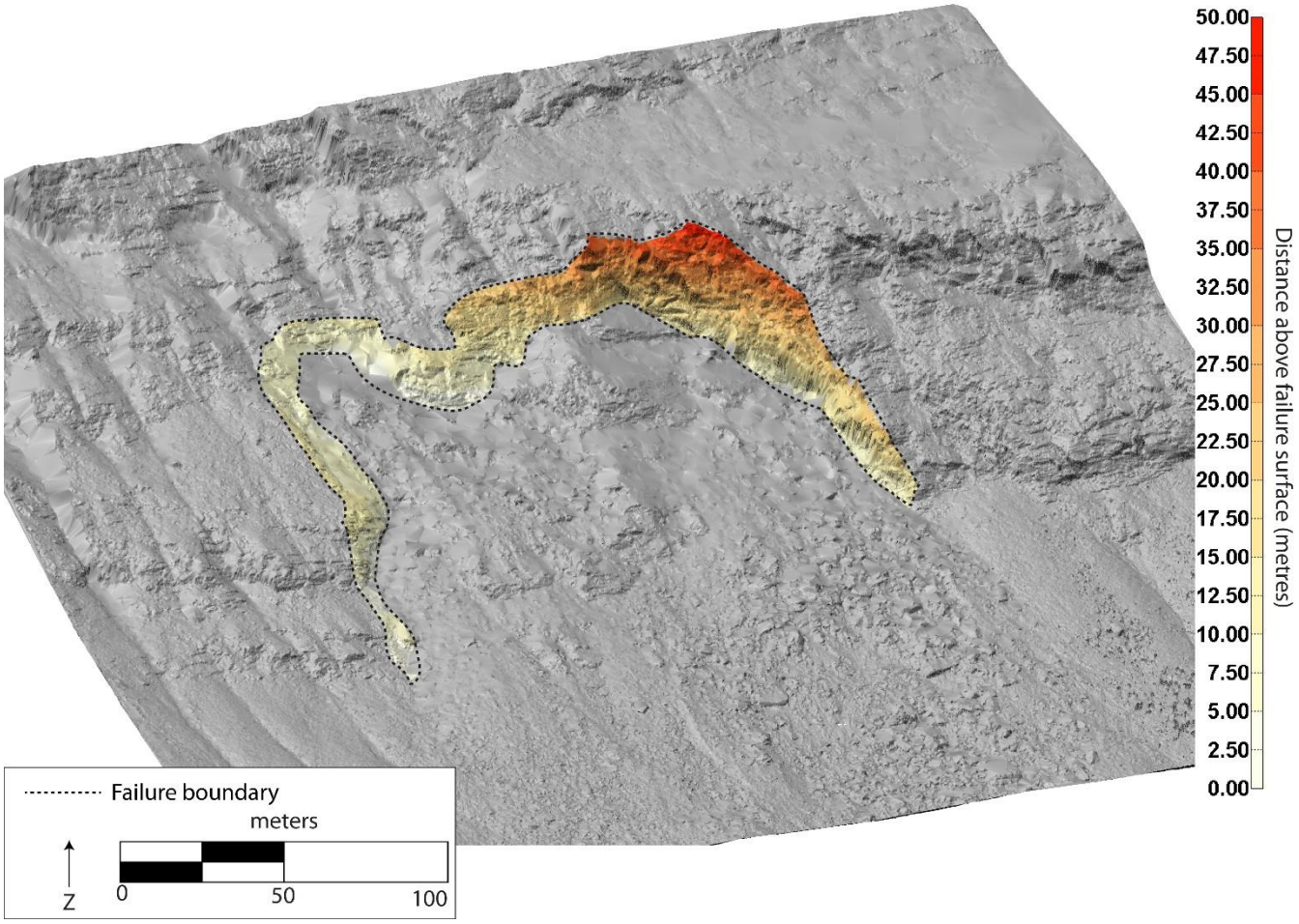

Figure 4. The failure zone of the Signaldalen rock avalanche (outlined with black stippled line) is a complex wedge much deeper to the plane of failure at its back than at the front. The colours indicate the distance in metres to the plane of failure (from white = 0 m to red = 50 m).

5

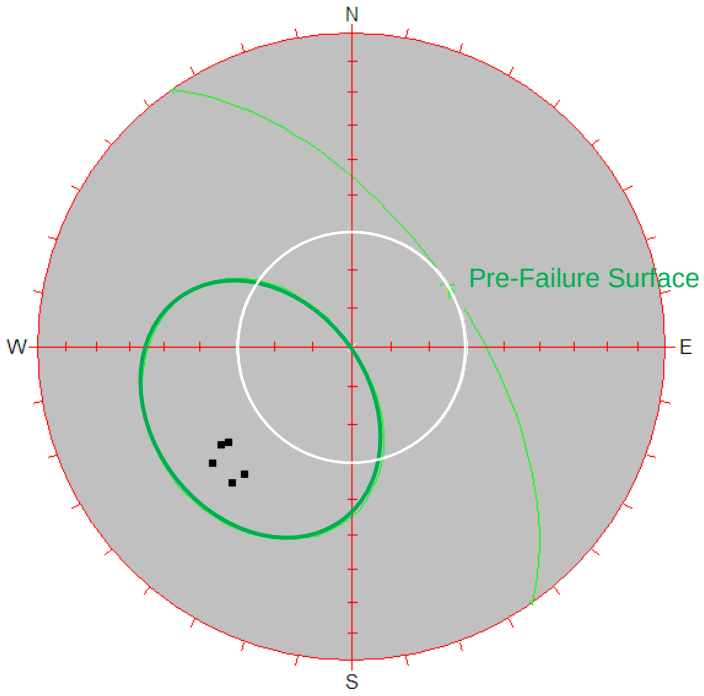

Figure 5. Kinematic analysis of the bedding planes for the sliding failure. The green line represents the orientation of the natural slope surface before failure, the white circle represents an estimated friction cone of 30° and the green cone represents the sliding daylight window for the associated pre-failure surface, the poles to the bedding surface are plotted as black markers.

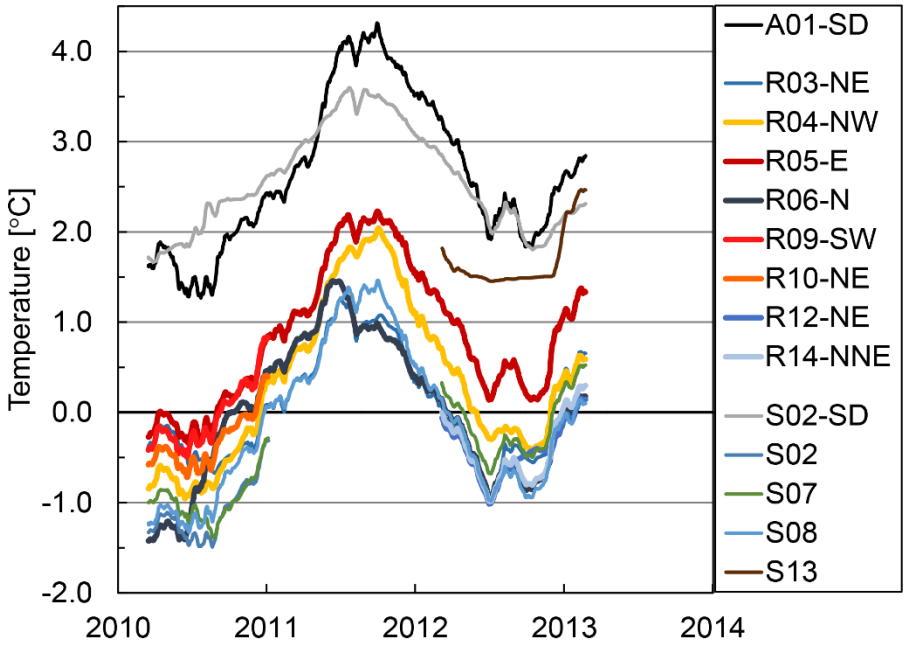

Figure 6. Mean annual rock- and soil surface temperatures (all except A01-SD) and air temperature (A01-SD) during the period Sept. 2009 to Aug. 2013 shown as simple moving 365-days average for all sites. To ensure that the temperature variability was not shifted in time, the mean values were centered (an equal number of days on either side of the mean value). A01-SD is air temperature in Signaldalen (SD), R03 to R14 are the rock face loggers and S02 to S13 are the soil temperature loggers.

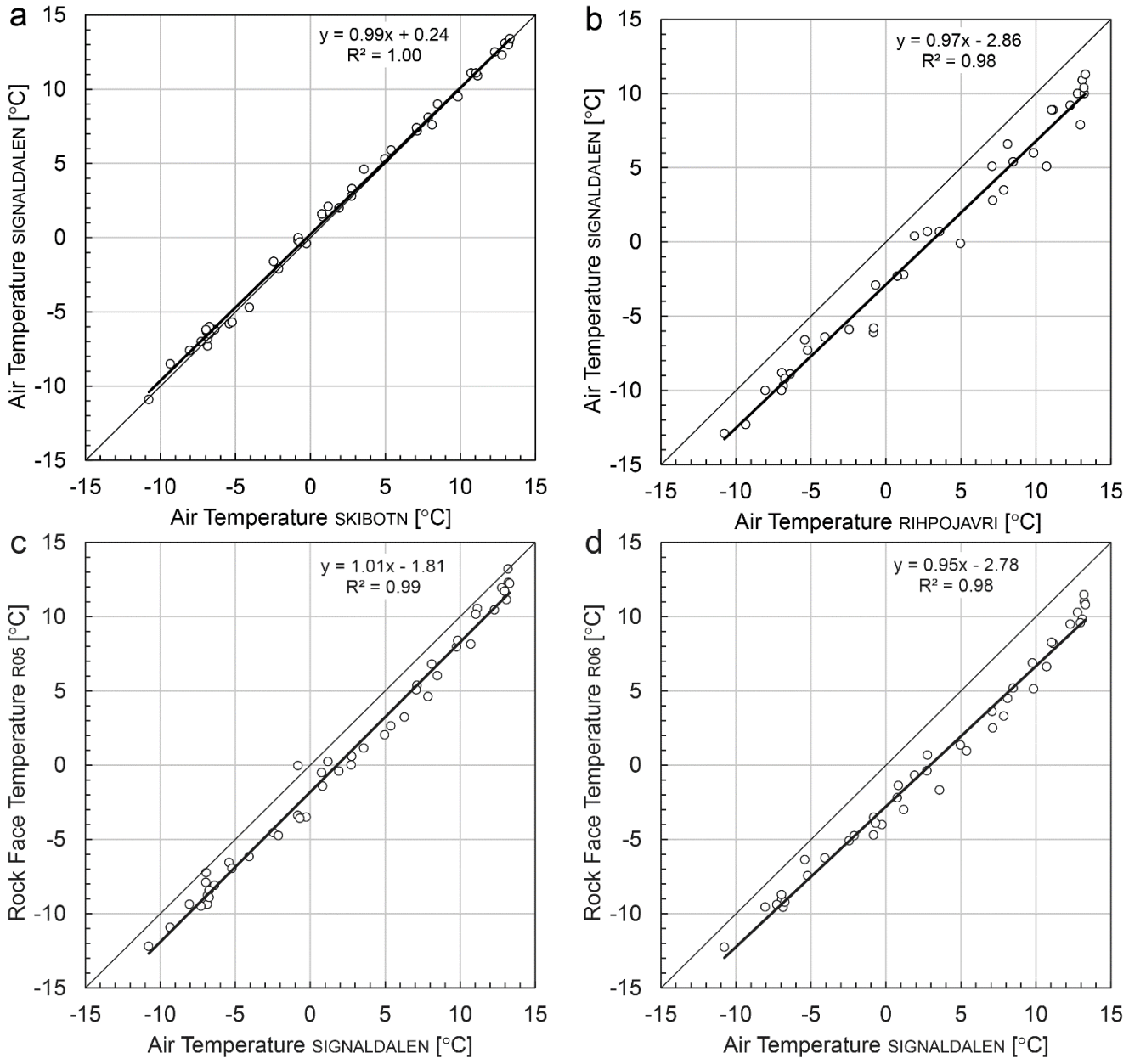

Figure 7. Scatter diagrams showing relations between monthly mean temperature for the main air temperature and rock face temperature series, including linear regression lines. (a) Relation between air temperature in Signaldalen and at meteorological station at Skibotn; (b) relation between air temperature in Signaldalen and air temperature measured at Rihpojavri weather station (25 km from Signaldalen); (c) and (d) relation between rock face temperature at logger site R05, respectively logger site R06 and air temperature in Signaldalen.

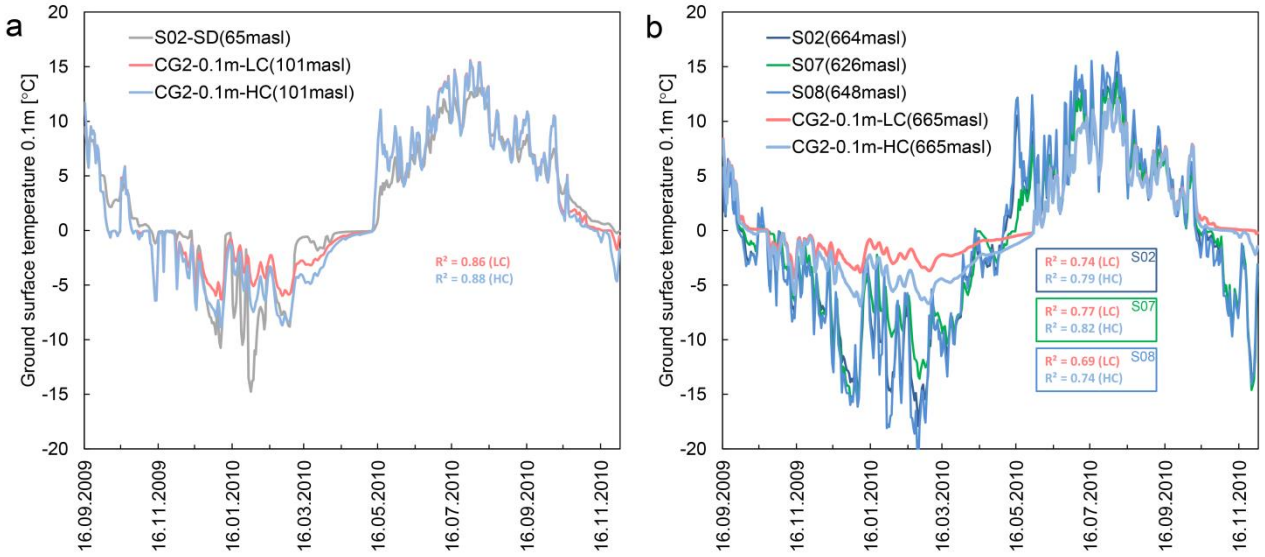

Figure 8. One year of observed soil surface temperatures (SST) at sites with an established soil and snow cover compared with the modelled SST from the transient permafrost model CryoGrid2 (CG2) for high (HC) and low (LC) thermal conductivity of the snow: a) time series of SST at site S02 – placed next to the air temperature measurement location in the valley floor – compared to the modelled CG2 series for the actual grid cell; b) SST series for the soil sites close to the release area (S02, S07 and S08) compared to the corresponding grid cell with similar elevation as the release area (i.e., 665 m asl).

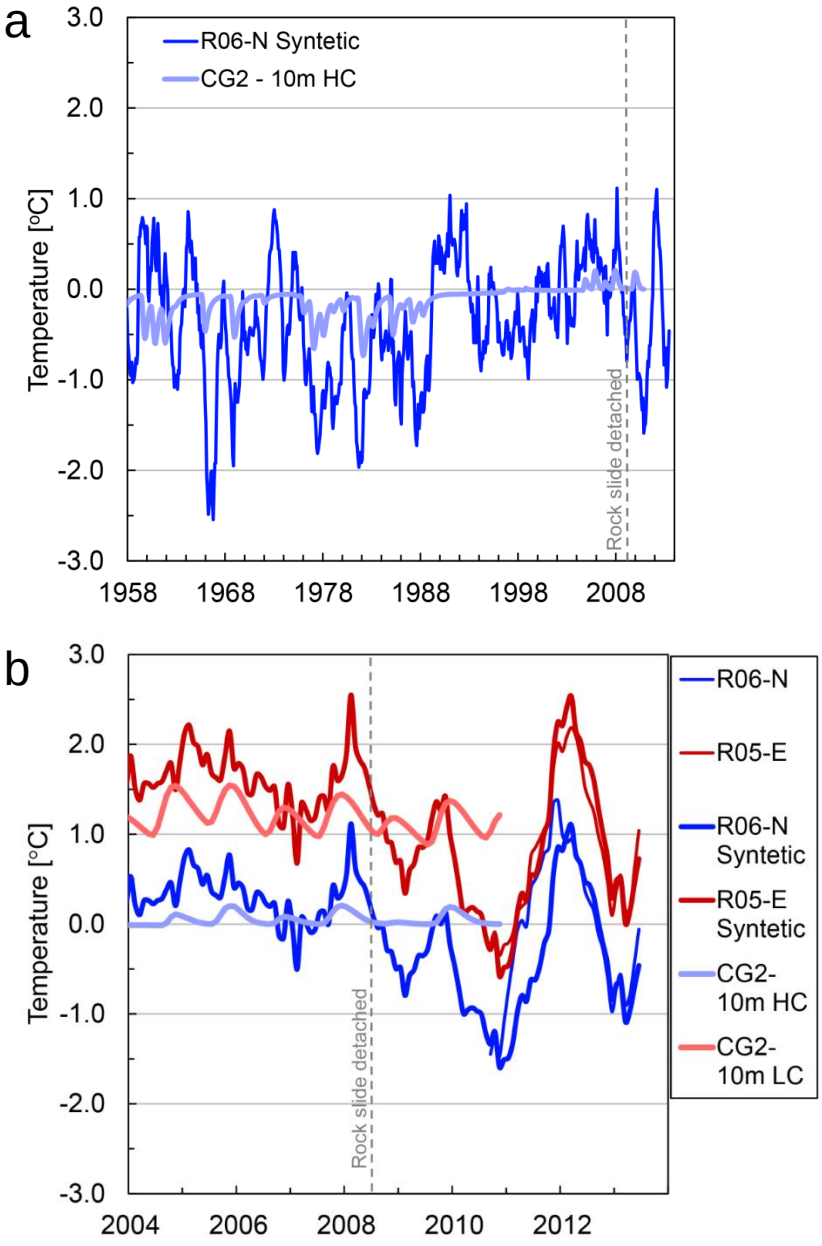

Figure 9. a) Synthetic series since 1958 of the coldest rock wall site (R06) based on the regression presented in Figure 7. Also shown is the transient permafrost model CryoGrid2 (CG2) run that calculates ground temperatures at 10 m depth according to conductive heat transfer in the soil and in the snowpack (Westermann et al., 2013). The CG2 model results are representative for areas at approximately 665 m asl with slope gradients allowing for snow accumulation. The grey dotted line shows when the Signaldalen rock avalanche detached; b) The recent 10-year period for the synthetic series overlaid on the respective in-situ RST data for the lowest (R06, blue lines) and highest (R05, red lines) rock wall temperatures. Also shown are the CG2 model data runs at 10 m depth for High (HC) and Low (LC) thermal conductivity of the snow.

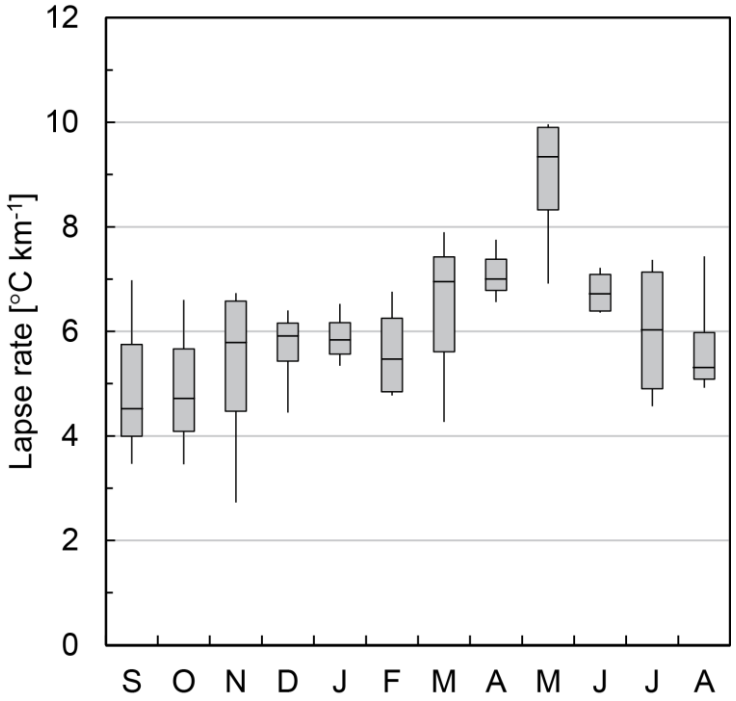

Figure 10. Inter-annual variability from 2009-2013 in monthly-mean lapse rates based on air temperature data from Rihpojavri (502 m asl) and Signaldalen (65 m asl) from 2009-2013. Boxes show the interquartile range of the month's lapse rate, horizontal lines inside the boxes show the median values, and the whiskers show the full range of the data.

5

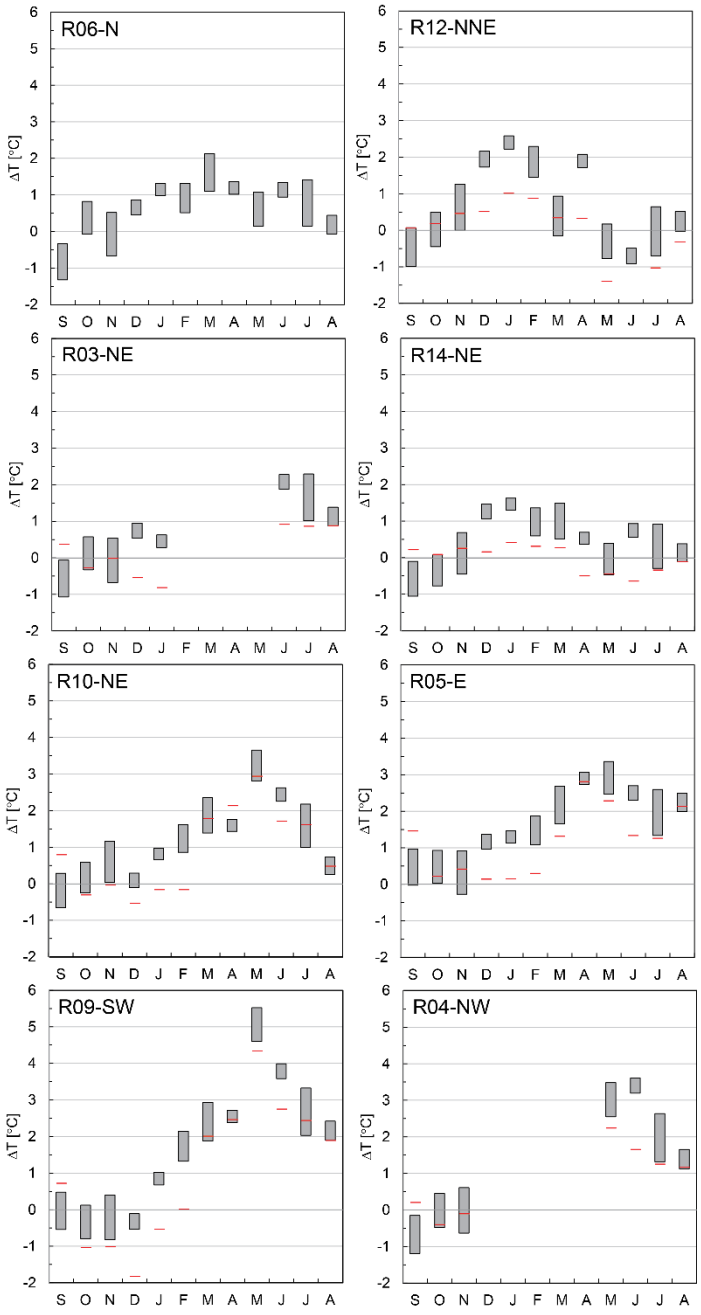

Figure 11. Monthly temperature difference (ΔT) between calculated air temperature and measured rock face temperatures from 2009-2013. Calculated air temperature is based on air temperature from Signaldalen (65 m asl) and lapse rates shown in Figure 9. Boxes show the interquartile range of ΔT. The red horizontal lines show the monthly-mean temperature difference between the respective loggers and the north-facing (i.e., the coldest) logger R06. Loggers R03, R04 and R12 were snow covered during winter and data was removed for snow-influenced months. For R09 and R10 only data for 2009-2011 exist, for R12 and R14 only for 2011-2013.

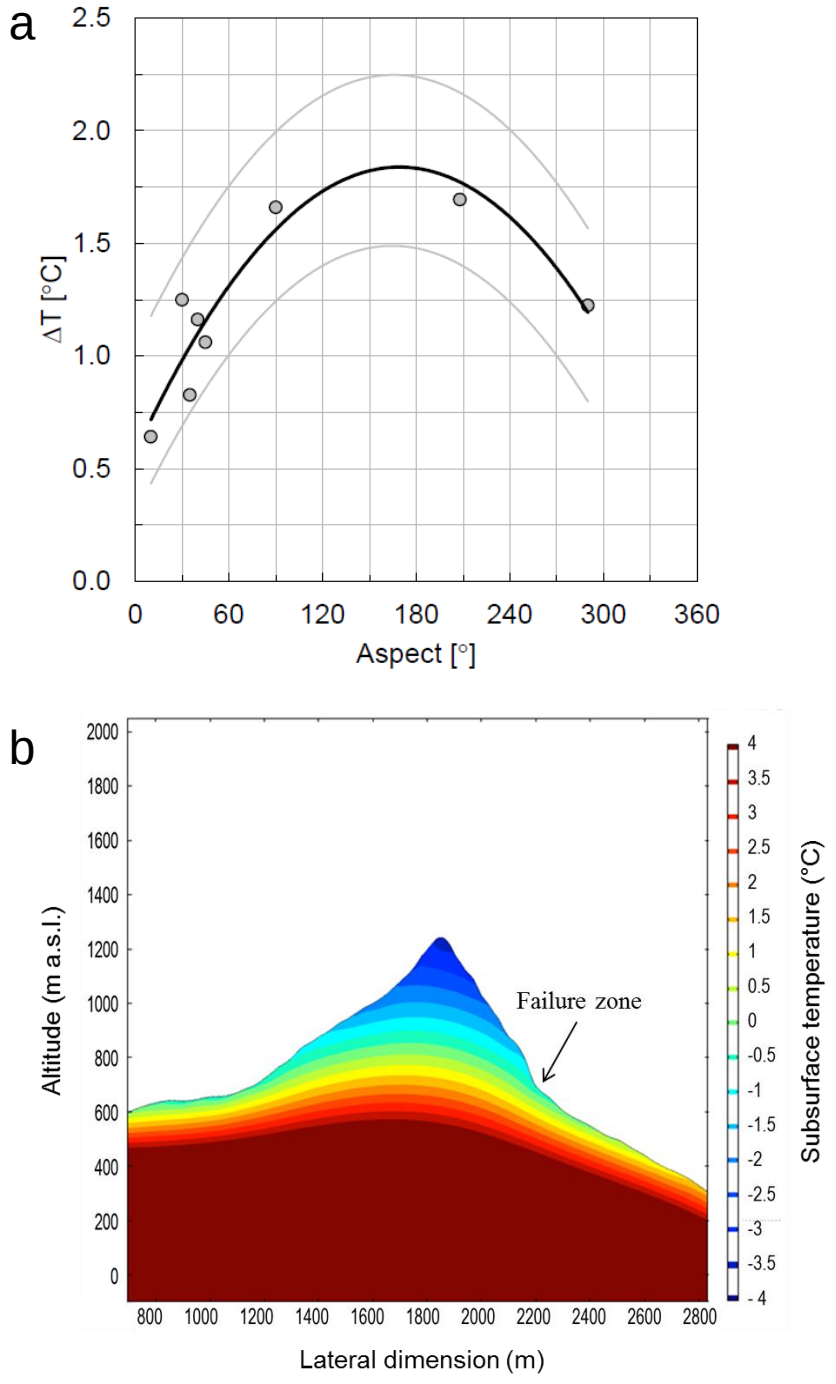

Figure 12. a) Annual temperature difference (ΔT) between calculated air temperature and measured rock face temperatures and aspect dependency as derived from the rock wall temperature data. The points represent the mean values and the black line is the best polynomial fit to the data (R^2=0.84). The grey lines show the polynomial fit to the interquartile range of ΔT; b) 3D transient heat modelling of the subsurface temperature field based on values identified in a). Figure shows a slice transecting the mountain from South (left) to North (right).

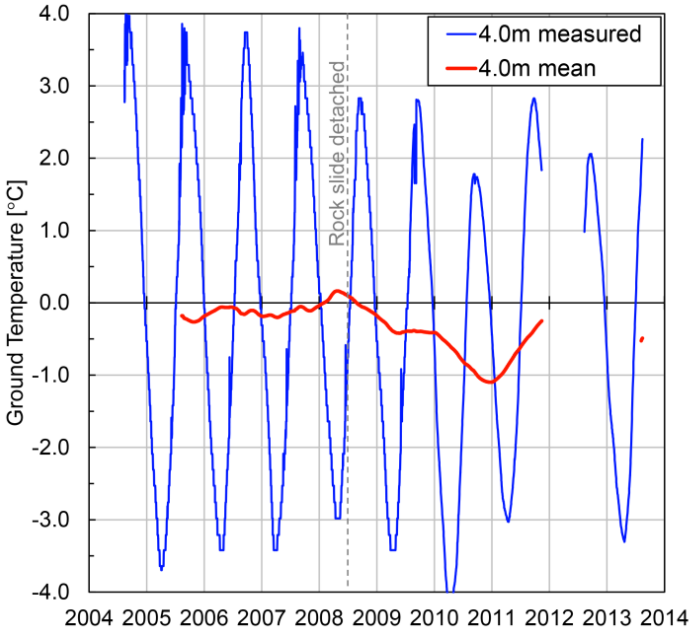

Figure 13. Ground temperature time-series at 4 m depth from a nearby permafrost borehole (Guolasjávri (Gu-B-1), 786 m asl; more details can be found in Farbrot et al., 2013). The blue line shows the measured daily values and the red line shows a simple moving 365-days average, i.e. the unweighted mean of the previous 365 days. The grey dotted line indicates the release date of the Signaldalen rock avalanche.